ACS OMEGA

Open Access

http://pubs.acs.org/journal/acsodf

Article

Characterization of the Mechanical, Biodegradation, and Morphological Properties of NBR/Biopolymer Blend, Integrated with a Risk Evaluation

Niloofar Akbarian-Saravi, Ibrahim Alper Basar, Olivia Helena Margoto, Nadia Abdollahi G, Bryn Crawford, Benjamin Magel, Mehrdad Gharibnavaz, Cigdem Eskicioglu,* and Abbas S. Milani*

Cite This: *ACS Omega* 2024, 9, 9256−9268

Read Online

ACCESS | Metrics & More | Article Recommendations | Supporting Information

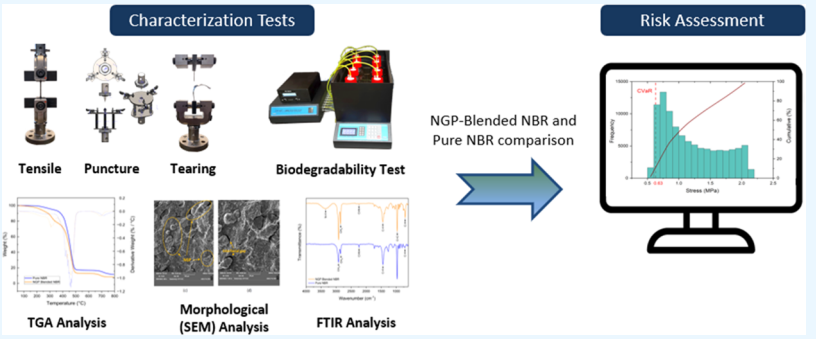

ABSTRACT: Biopolymer blends have attracted considerable attention in industrial applications due to their notable mechanical properties and biodegradability. This work delves into the innovative combination of butadiene-acrylonitrile (referred to as NBR) with a pectin-based biopolymer (NGP) at a 90:10 mass ratio through a detailed analysis employing mechanical characterization, Fourier transform infrared (FTIR) analysis, thermogravimetric analysis (TGA), and morphology studies using SEM. Additionally, biopolymer's biodegradability under aerobic and anaerobic conditions is tested. The study's findings underscore the superior tensile strength and elongation at break of the NGP/NBR blend in comparison to pure NBR, while also exhibiting a decrease in puncture resistance due to imperfect bonds at the particle−matrix interfaces, necessitating the use of a compatibilizer. In anaerobic conditions, evaluation of biodegradable properties reveals 2% and 12% biodegradability in NBR and NGP/NBR blend, respectively. The degradation properties were also aligned with TGA results highlighting a lower decomposition temperature for NGP. Additionally, this research integrates the application of a conditional value-at-risk (CVaR)-based analysis of the blend's tensile properties to evaluate the uncertainty impact in the experiment. Under risk, a significant enhancement in the tensile performance (by 80%) of the NGP/NBR blend was shown compared to pure NBR. Ultimately, the study shows that adding pectin to the NBR compound amplifies the overall performance of the biopolymer significantly under select criteria.

1. INTRODUCTION

Recent trends in global plastics consumption have led to a proliferation of studies focusing on biodegradable resources as a replacement for conventional plastic products. Annual production of plastics is expected to reach >590 million metric tons by 2050, leading to substantial environmental pollution. In this regard, the development of natural renewable biodegradable plastic resources is an increasing area of academic and industrial research priorities.[1] Next to blending new biodegradable plastics, recent studies have focused on biodegradable elastomeric materials based on nitrile, butadiene nitrile, and natural rubber.[2−4] Elastomers such as natural rubber and synthetic rubber are a special class of polymers, characterized by both high viscoelasticity and weak intermolecular interactions.[5] Compared to other elastomeric materials, rubber poses exceptional mechanical properties due to the cross-linking reactions in unsaturated bonds. High elasticity, low compression set, high elongation, and high tensile and tear strengths are among the desired properties of vulcanized rubber. As a result, this material is widely used in industrial applications ranging from tires and hoses to gloves and many others.[6−8]

Nitrile rubber (NBR) is a polar elastomer with high resistance to hydrocarbon oils. However, it suffers from a

Received: October 22, 2023
Revised: January 17, 2024
Accepted: January 24, 2024
Published: February 13, 2024

relatively low modulus and strength.[9,10] In recent decades, researchers have sought to develop rubber-based blends of polymers to combine advantageous properties of the individual components. Such improved properties encompass mechanical properties, processability, and biodegradability. Kwak and Nakajima[11] blended acrylonitrile copolymer (NBR) and poly(vinyl chloride) (PVC) and suggested a schematic model for its homogenization mechanism. The properties of the mixture of NBR and polychloroprene rubber (CR) were investigated by Botros et al.[12] Wimolmala et al.[13] combined PVC and NBR at various rubber-to-plastic ratios. They concluded that the blend with a 30% rubber composition had the highest tensile toughness among the samples they tested. A major disadvantage of the mentioned petroleum-based polymers' blending with NBR, however, is linked to their nonrenewability and nonbiodegradability.[14]

The drastic increase in the use of rubber-based personal protective equipment (PPE) during the SARS-CoV-2 pandemic also revealed that we are in imperative need of developing more sustainable and environmentally friendly rubber-based disposable PPE. An environmentally friendly rubber material can be achieved by using biopolymers in the blends. Biopolymers are often categorized based on three sources:[9] (1) natural fibers, (2) bioderived monomers, and (3) microbial biopolymers. Natural fibers, the most abundant sources of biobased polymers, with low density and low cost, include cellulose, hemicellulose, lignin, and pectin.[15,16] Among natural fibers, pectin, known as a main binder of the fiber cell wall and polysaccharide, has not been widely investigated in rubber-based biopolymer blends.[9,17] Pectin can be extracted and utilized as a water-soluble anionic biopolymer. Numerous recent studies underscore the benefits of employing pectin as a biopolymer, including serving as a thickening and gelling agent, colloidal stabilizer, texturizer, and emulsifier.[18−21] Specifically, the acetyl and methoxyl groups in pectin are hydrophobic, which can explain its emulsifying capabilities.[22,23]

It is worth noting that blending nitrile rubber with a chemically incompatible component can potentially lead to an adverse mechanical effect (poor mechanical properties of the blend), despite reducing the environmental and economic concerns.[24−26] Past investigations have been carried out on biopolymer/polymer blended nitrile rubber and analyzed the ensuing effective physical properties.[27,28] Boukfessa and Bezzazi[9] investigated the effect of using fillers in the blended natural rubber and NBR on the ensuing tensile and tear strengths. More recently, Nihmath and Ramesan[29] investigated chlorinated NBR blended with chlorinated ethylene propylene diene rubber and analyzed the effect of the blend ratio on the ensuing tensile strength, tear resistance, and elongation at break. Considering the biosource aspect, more recently, Jantachum et al.[30] analyzed the effect of using cellulose nanocrystals on the properties of NBR and natural rubber composition. The study revealed improved processability in the rubber nanocomposites, attributed to the utilization of cellulose-based additives. While reinforcing fillers have been extensively used in rubber to improve its mechanical properties,[31] to the best of the authors' knowledge, in the context of rubber-based polymer blends, no earlier study examined the impact of pectin as a biobased filler on NBR multicharacteristics including mechanical properties, biodegradability enhancement, interphase adhesion, etc.

When designing a new material including green blends, the incorporation of risk management methods such as Value at Risk (VaR) and Conditional Value at Risk (CVaR) can also be beneficial, namely, to ensure the new materials' robust performance in practice. Recent works have borrowed the VaR and CVaR from their original application area (Finance) and applied them in engineering areas. For instance, Li et al.[32] proposed an innovative method based on the CVaR and used it for a design optimization process via gradient-based Monte Carlo (MC) simulations. In the present study, to investigate the potential variability of the stress−strain behavior of the new NBR/NGP blend, the CVaR analysis is also employed (more details are presented in Section 2.4).

1.1. Objective. This study aims at blending and characterizing an NBR (90 wt %) fabricated with NGP (10 wt %), while also considering potential variation (uncertainty) in the blend material's performance for industrial applications. The NBR is composed of acrylonitrile (35 wt %), methacrylic acid (25 wt %), and 1,3-butadiene (40 wt %), while the NGP additive as a biosource consists of 80 wt % base polymer, 6 wt % pectin, and 14 wt % other ingredients (e.g., bentonite, iron oxide). Specifically, the work tackles:

- Conducting mechanical tests on the NGP (10 wt %)-blended NBR (90 wt %) as compared to the pure NBR; including tensile strength, tear strength, elongation at break, and resistance to puncture, followed by respirometric aerobic and anaerobic biodegradability evaluations.
- Performing Fourier transform infrared (FT-IR) spectroscopy, morphological analysis, and thermogravimetric analysis (TGA) to analyze functional groups in the above blends and characterize their compositions, microstructure, and thermal performances.
- Applying a MC-based risk analysis to calculate the CVaR for both materials, and thereby comparing their expected performance in the presence of potentially varying tensile response.

1.1.1. Novelty. Aligned with the wide industrial interest in manufacturing new biopolymer/NBR blend materials (e.g., toward new green PPE), the present work for the first time studies a pectin-based biopolymer (NGP) blended with NBR and evaluates its performance mechanically and environmentally. Moreover, most previous studies reviewed in Section 1 focused on common mechanical properties such as tensile strength, tear strength, and elongation at break. There has been a lack of measuring puncture resistance for such elastomeric materials especially when they are aimed for use in PPE such as gloves. In addition, a risk analysis method is proposed here for the first time to address potential uncertainties in characterization factors during tensile testing, or due to the variation of the applied load to the material in service.

The rest of the manuscript has been organized as follows. In Section 2, the selected materials and the proposed methodology are outlined. Results and discussions are presented in Section 3, followed by the concluding remarks in Section 4.

2. MATERIALS AND METHODS

We used the NBR as the base material. We initially obtained NBR from two different sources (for comparison and final selection in the present blending application): Kumho Petrochemical (KP) (South Korea) with 35% acrylic content and Nitriflex (NF) (SP, Brazil) with 33% acrylic content. NBR is nominally composed of acrylonitrile (35 wt %), methacrylic acid (25 wt %), and 1,3-butadiene (40 wt %) in an aqueous

https://doi.org/10.1021/acsomega.3c08301
ACS Omega 2024, 9, 9256−9268

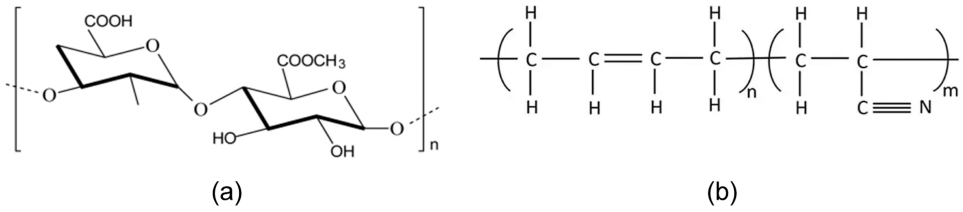

Figure 1. Illustration of the NGP/NBR blend mechanism employed to produce biopolymer: (a) pectin-based NGP; (b) NBR (Photograph courtesy of Kitir et al.[34] and Mao et al.,[35] Copyright 2023).

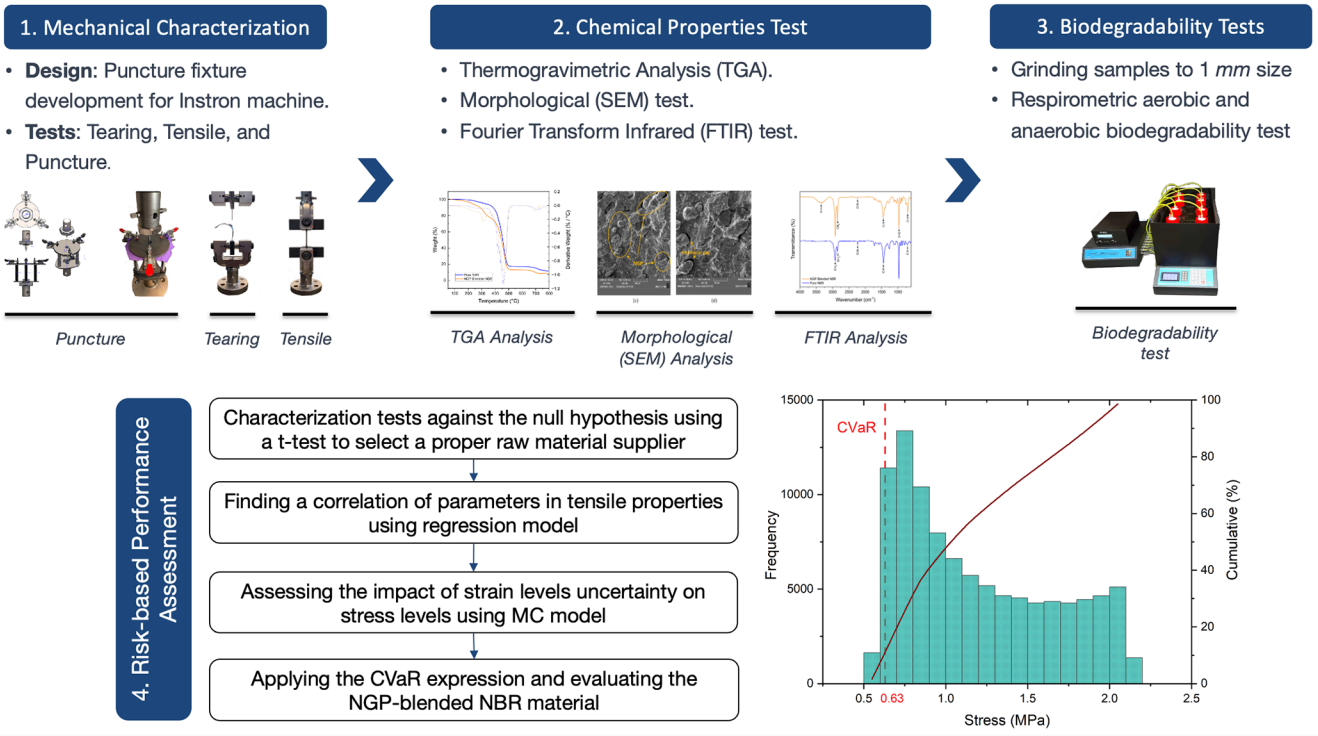

Figure 2. Overview of the employed methodology including mechanical, composition/blend, biodegradability, and performance risk analyses.

emulsion with the presence of an emulsifier. For the NGP-blended NBR, we dispersed the NGP additive (10 wt %, provided by Feed Engineering, Inc.) as a biobased polymer composed of around 80 wt % base polymer, 6 wt % pectin, and 14 wt % additional components such as bentonite, iron oxide in a solvent (water/alcohol), which is compatible with polymers. Then, the dispersion solution was processed to be evaporated. Following, the dispersed NGP was added to NBR and the samples (10 wt % NGP and 90 wt % NBR blend) were prepared in the form of thin films (<2 mm thick) by casting process and at a reaction temperature near 160−170 °C using an oven. Thus, the vulcanization of the NGP/NBR blend took place by the endothermic reaction.[33] The chemical structure of NGP/NBR is shown in Figure 1. Figure 2 depicts the overview of the evaluation methods used to compare the NGP-blended NBR and pure NBR samples, comprising mechanical, morphological, chemical composition, and biodegradation characterization tests. All experiments were conducted in triplicate. For brevity, details of each experimental setup are presented in Appendix A in the Supporting Information.

2.1. Morphology (SEM). Morphological evaluations of freeze-fractured specimens were conducted using a TESCAN MIRA3 microscope, employing a beam intensity of 15 kV and maintaining a working distance of 15 mm. Prior to imaging, the specimens underwent a platinum coating process with a thickness of 20 nm.

2.2. Thermogravimetric Analysis (TGA). Thermogravimetric analysis (TGA) was performed utilizing the TA Instruments TGA550 under controlled test conditions. The test environment was maintained with a continuous flow of nitrogen gas at a rate of 25 mL/min. The samples were subjected to gradual heating, with the temperature increasing at a rate of 10 °C/min, ranging from an initial temperature of 30 °C to a maximum of 800 °C.

2.3. Fourier Transform Infrared (FT-IR) Analysis. The characterization of functional groups within the samples was accomplished through Fourier transform infrared-attenuated total reflection (FTIR-ATR) spectroscopy as a qualitative technique widely used in the polymers industry, which can easily identify raw rubbers.[36] The analysis was conducted using a Thermo Scientific Nicolet iS20 instrument, sourced from Thermo Fisher Scientific. The FTIR-ATR spectra were acquired across the spectral range of 4000 to 500 cm^{-1}, with each spectrum comprising 32 scans, and a spectral resolution of 16 cm^{-1}.

2.4. Risk-Based Performance Evaluation Model. Upon completing experimental characterization tests, a risk analysis method was adapted to compare the two material groups for

https://doi.org/10.1021/acsomega.3c08301
ACS Omega 2024, 9, 9256−9268

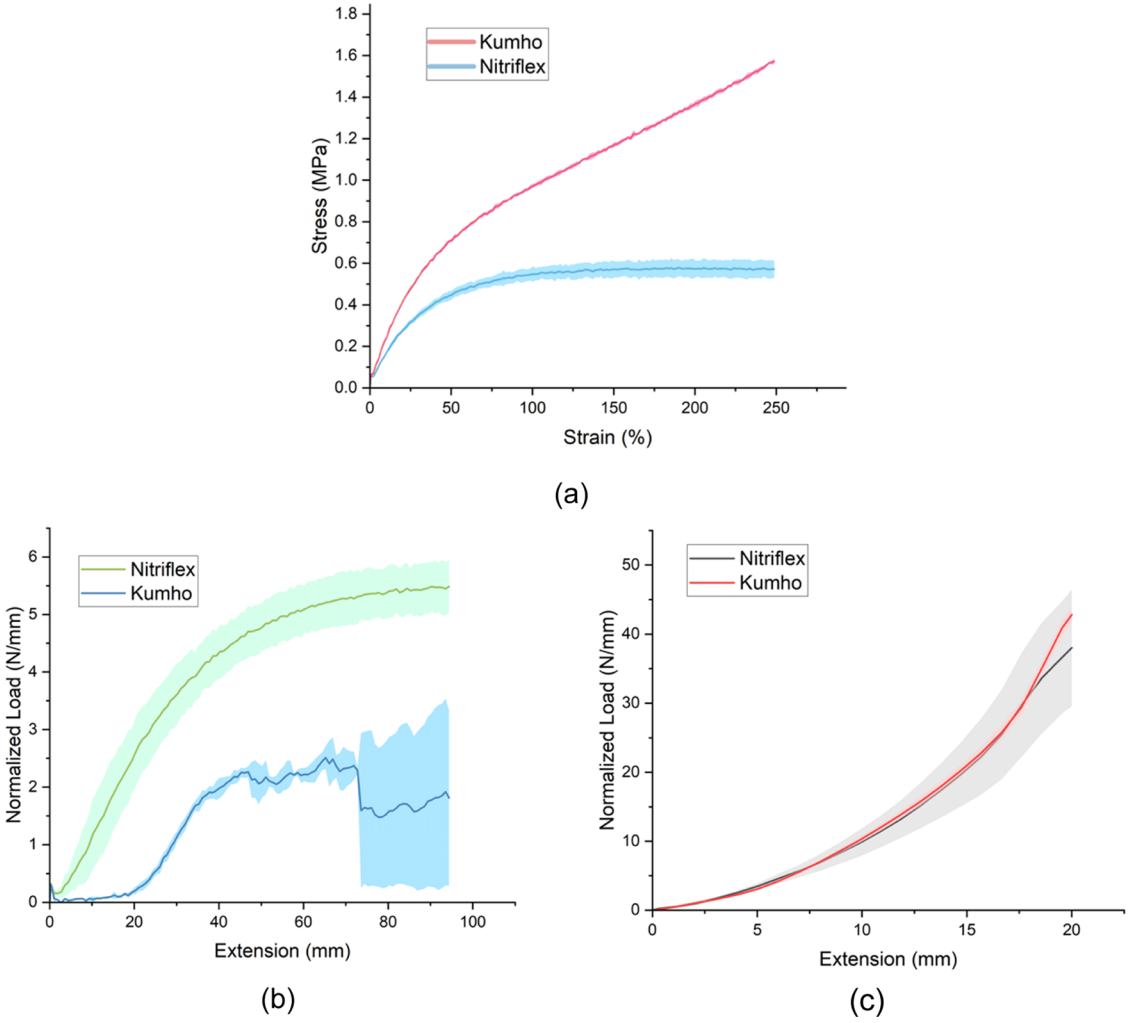

Figure 3. Mechanical properties comparison of the two base NBR materials: (a) tensile testing, (b) tear testing, and (c) puncture testing.

Table 1. Comparison of the Ultimate Strength in MPa (and the Corresponding Strain% at Break; Shown in Parentheses) of the NGP-Blended NBR and Pure NBR

	n	1	2	3	mean	STD
NGP-blended NBR	3	2.44 (502)	2.2 (545)	2.70 (473)	2.45 (506)	0.25 (36)
Pure NBR	3	1.74 (287)	1.98 (327)	2.88 (460)	2.20 (358)	0.60 (90)

their tensile performance reliability. Namely, to evaluate the impact of potential uncertainties in the materials' performance, e.g., due to potential variations during blending or varying in-service conditions, etc., a probabilistic analysis was carried out using the regression-based MC simulation. To generate statistical samples from a range of tensile strain (extension) levels, a uniform distribution was assumed. The extension level and average stress level of each material were fitted using a polynomial regression and then used in the MC simulation. For the latter, the number of iterations was calculated using[37]

$$N = \left(\frac{Z \times \sigma}{\varepsilon \times \mu}\right)^2 \quad (1)$$

where N is the number of iterations, σ and μ are the standard deviation and the mean value of the model's output (here tensile stress), respectively, ε is the maximum allowable marginal error, and Z is the minimum required confidence interval of the two-tailed normal distribution. Based on the mean value and the standard deviation of the output using 1500 random iterations, and assuming a marginal error of 0.05%, the number of required iterations was estimated to be 100,000.

Theoretically, the VaR represents the worst-case output probability, given the specified confidence $(1 - \alpha)$. On the other hand, CVaR is the extended risk measure of the VAR, by measuring the accumulative level of the expected outcome if the worst-case threshold (α) is ever crossed, as follows[37]

$$\text{stress level at risk}_\alpha(X) = \text{INF}\{x \in R: F_X(X) > \alpha\} \quad (2)$$

$$\text{CVaR} = \frac{1}{1-\alpha}\int_{-1}^{\text{VaR}} x \cdot p(x)\mathrm{d}x \quad (3)$$

where F_X is the cumulative probability distribution function of the stress level x (derived from the output of the MC simulation model) and $(1 - \alpha)$ is the confidence level. In other words, here, CVaR represents the tensile stress level that the material can produce in $100(1 - \alpha)\%$ of the times under

https://doi.org/10.1021/acsomega.3c08301
ACS Omega 2024, 9, 9256−9268

uncertainty. $p(x)$ is the probability density of getting an outcome with value x. The confidence level for VaR and CVaR is commonly set at 95 or 99%[38] (here, it is assumed to be 95%). When comparing the two materials' average stress–strain curves, two-way ANOVA was also conducted to further evaluate and support the results of the above CVaR analysis.

3. RESULTS AND DISCUSSION

3.1. NBR Source Effect. The mechanical properties of the two different base nitrile materials, acquired from KP and NF, were compared; given the average sample thicknesses of 1.77 mm (KP) and 2 mm (NF). For the tensile properties, the KP material resisted a higher loading compared to the NF, given the same strain level (250%; Figure 3a). On average, the KP material had a 250% higher ultimate strength, presumably due to the higher acrylic content (Section 2).

As shown in Figure 3b, with respect to the tear resistance, both tearing force and elongation at break were greater for the NF specimens compared to KP. Finally, with respect to the puncture resistance, shown in Figure 3c, both types of NBR samples showed an average of ~40 N/mm under 20 mm extension, but the KP specimens had much less variation through the test repeats. To statistically evaluate the difference in NF and KP samples at the extreme puncture state, a *t*-test was performed using ultimate force values, considering 3 test repeats per material group.[39] It was found that the difference in the ultimate puncture resistance force values is not statistically significant (p-value > 0.05).[40] Note that in addition to the materials' stiffnesses (which were different based on Figure 3), surface roughness (R_a) and thickness also contributed to the friction, which in turn impacts the puncture resistance of the material.[41,42] Surface roughness is one of the most important features in the materials quality evaluation. Therefore, a three-dimensional (3D) optical microscope (model: Bruker Contour GT-K) was used to observe the surface quality of the sample, allowing roughness measurements to be made by means of multiple statistical measures including R_a (the arithmetic mean of the absolute values of the surface departures from the mean plane), R_p (the surface peak), and R_v (the surface pit/valleys). It was seen that the two raw materials' surfaces have similar roughness (i.e., $R_{a(KP)}$ = 4.42 μm, $R_{a(NF)}$ = 4.88 μm).

3.2. Mechanical Characterization of NGP-Blended NBR versus Pure NBR. Based on the previous section, the NBR by KP showed a higher tensile strength and less variation in puncture resistance (while being similar to NF under other measures); hence, it was selected as the final base NBR for blending with NGP and subsequent analysis.

According to Tables 1 and 2, on average, an 11% improvement in the ultimate strength and 15% improvement in the tearing resistance was noted for the NGP-blended NBR, compared to the pure NBR; however, given the large deviations in the tensile tests repeats after ~250% strain (i.e., toward ultimate strength points per Figure 4), the statistical significance levels were above 5%. In terms of the ultimate puncture resistance (Table 3 and Figure A7), there was a notable reduction (13%) in the maximum puncture force of the NGP-blended NBR compared to the NBR. To further analyze the difference in the materials characteristics, the surface roughness parameters were also calculated. As can be seen in Figure 6, and parametrized in Table A1 in the Supporting Information, the NGP-blended NBR showed a higher surface roughness (R_a) as compared to the pure NBR. This could partly explain the difference in puncture force

Table 2. Comparison of the Ultimate Tearing Resistance (N/mm) of the NGP-Blended NBR and Pure NBR

	n	1	2	3	mean	STD
NGP-blended NBR	3	3.19	3.06	3.62	3.29	1.38
Pure NBR	3	2.52	3.24	2.76	2.84	0.4

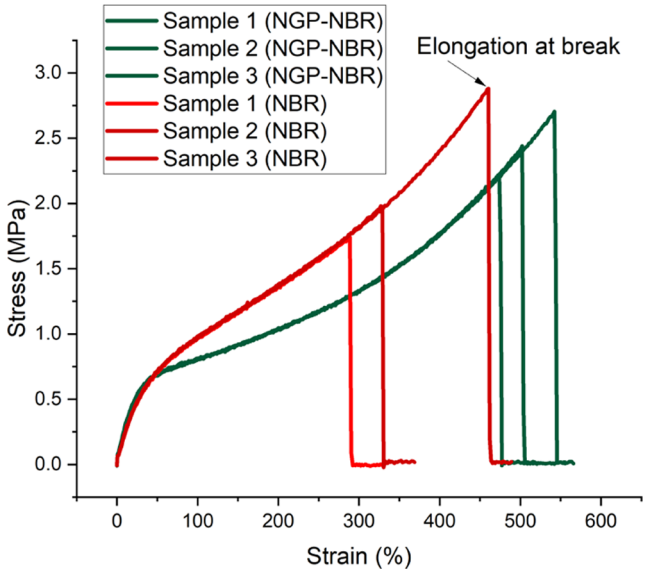

Figure 4. Comparing the full-range response of the pure NBR and NGP-blended NBR under tensile loading (note that up to ~250% strain, the repeatability of the two materials is excellent, while NGP-blended NBR continues to be robust at higher loading ranges).

Table 3. Comparison of the Maximum Puncture Resistance Force (N/mm) of the NGP-Blended NBR and Pure NBR

	n	1	2	3	mean	STD
NGP-blended NBR	4	37.7	37.42	35.91	36.48	1.38
Pure NBR	4	42.12	42.44	40.16	42.16	1.54

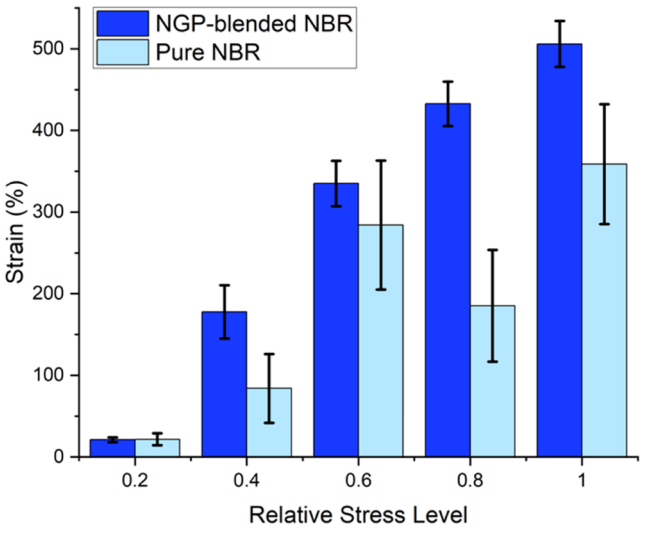

Figure 5. Average tensile strain% under different stress levels relative to the ultimate strength (e.g., inferring a safety margin during material's service).

https://doi.org/10.1021/acsomega.3c08301
ACS Omega 2024, 9, 9256−9268

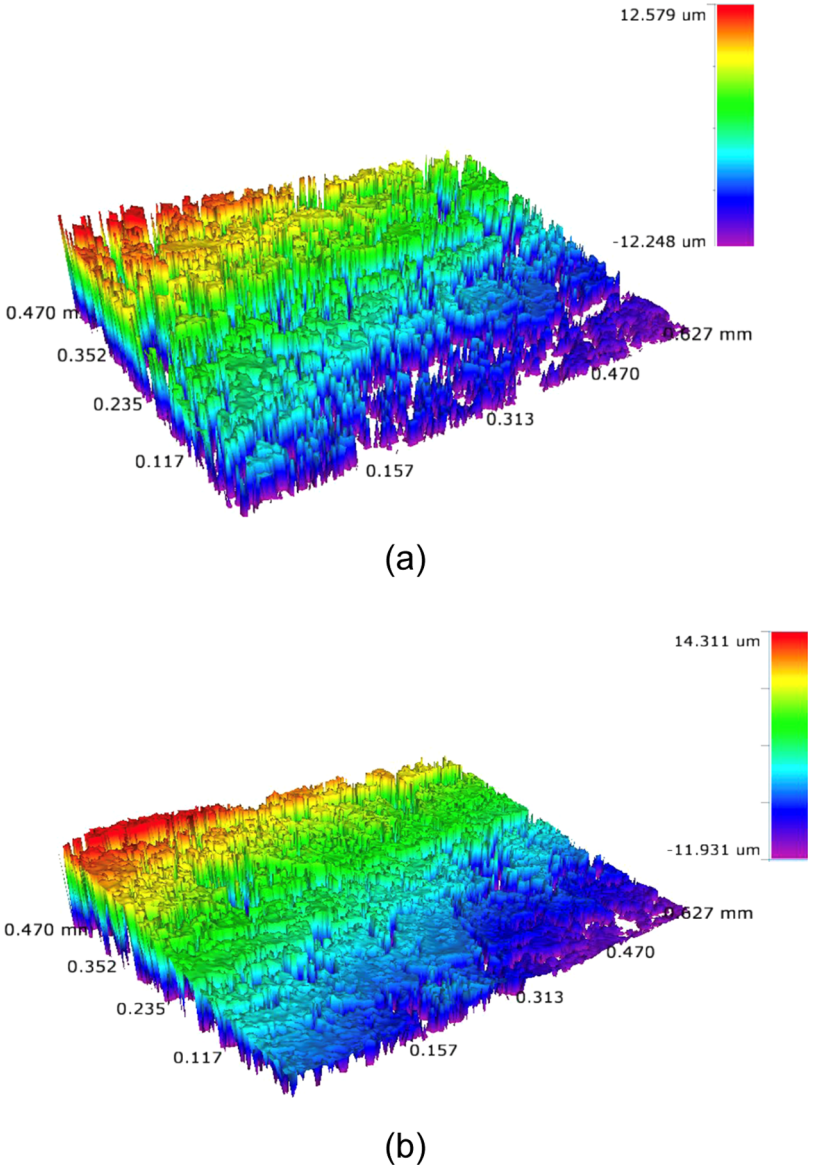

Figure 6. Topography of the samples using 3D optical microscope: (a) pure NBR (R_a: 4.42 μm); (b) NGP-blended NBR (R_a: 4.78 μm).

resistance between the two materials; however, it can be influenced by various other factors, such as other surface parameters, the material properties, as well as the geometry of the penetrating object. The elongation (tensile strain%) at break was notably higher in NGP-blended (506%) compared to NBR (358%), suggesting more stretchability when used, e.g., in a PPE such as protective glove. According to Figure 4, considering the same moderate level of target strain (e.g., up to 250%), the pure NBR outperformed the NGP-blended NBR, and both materials in this range have shown excellent relatability. A comparable elastic modulus was also seen for the two materials. At higher strain values close to breaking, however, the NGP-blended NBR revealed a more robust behavior.

In another type of comparative statistical analysis for the tensile response, one factor was assumed to be the level of applied stress relative to the ultimate strength, which would be selected in practice based on a given design requirements (Figure 5). The other factor (as the main treatment factor) was considered to be the material type, i.e., here with two levels (NGP-blended NBR and NBR, which equivalently accounts for the effect of the substitution of 10% of nitrile with NGP to pure NBR). As such, a two-way ANOVA was conducted, showing the significance of the material type factor (p-value < 5%). According to Figure 4, the NGP-blended NBR on average shows a 41% improvement in the corresponding elongation at break, in comparison to the pure NBR.

3.3. Morphological Analysis (SEM). The results of scanning electron microscopy (SEM) imaging, as illustrated in Figure 7, revealed the morphological characteristics of NBR and NBR blended with NGP. The SEM images supported the potential presence of oval-shaped NGP particles within the blended sample with high variations in particle sizes, though spanning the micron range, throughout the polymer matrix.

SEM analysis unveiled that the NGP particles do not have perfect adhesion to the polymer matrix. Instead, discernible gaps appeared at the interfaces between the NGP particles and the NBR matrix that might be related to NGP, as depicted in Figure 7c,d. These findings, which were validated through material expert opinion, resonated also with the earlier

https://doi.org/10.1021/acsomega.3c08301
ACS Omega 2024, 9, 9256−9268

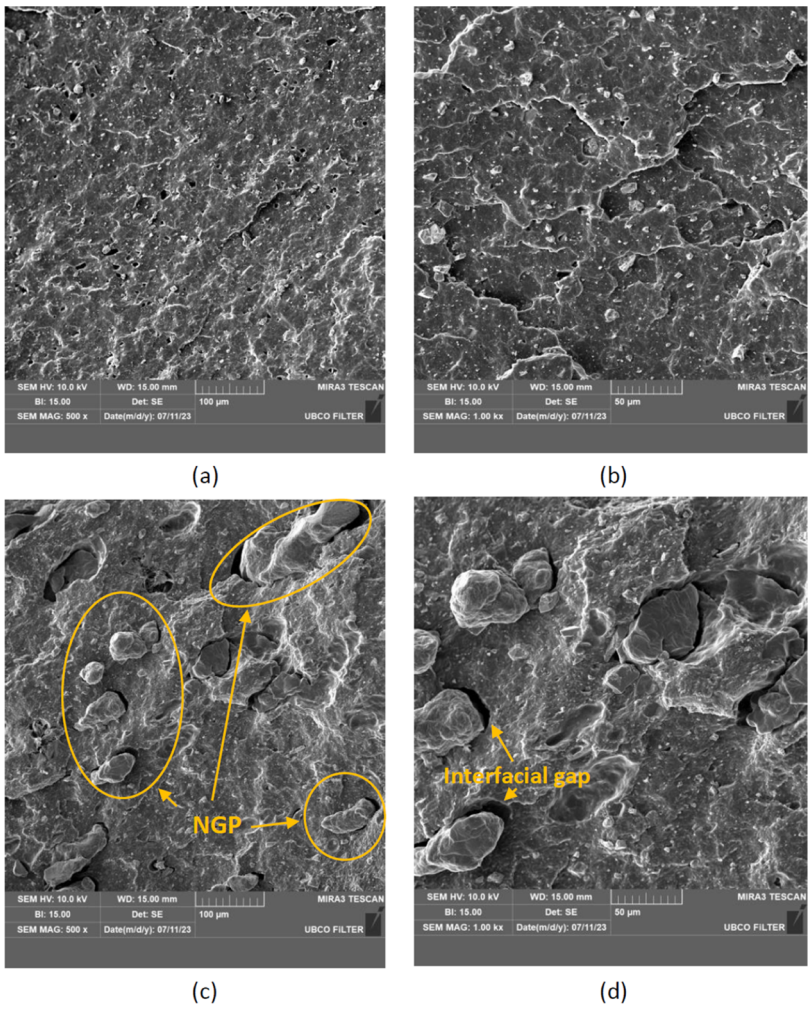

Figure 7. SEM morphology of (a) pure NBR at 500×, (b) pure NBR at 1k×, (c) NGP-blended NBR at 500×, and (d) NGP-blended NBR at 1k× magnifications.

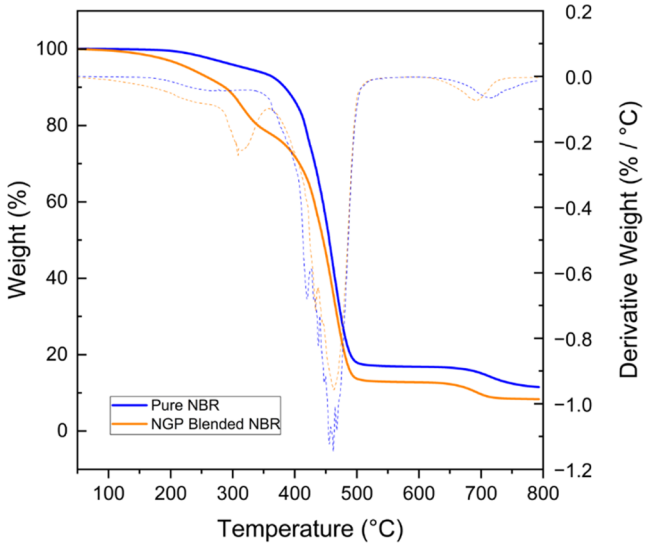

Figure 8. TGA results of pure NBR and NGP-blended NBR.

outcomes of the puncture test, where the NGP-blended samples exhibited inferior puncture resistance compared to pure NBR along with higher surface roughness. The addition of a compatibilizer/filler can serve as a strategy to bridge the gap between these two materials, promoting enhanced compatibility and consequently improving the overall properties of the composite.[43−46] The filler can be particularly situated at the boundary between the distinct polymers, promoting compatibility within the otherwise immiscible blend.[47,48]

Table 4. TGA Test Results

sample	pure NBR	NGP-blended NBR
$T_{5\%}$ (°C)	321	229
T_{dmax1} (°C)		307
T_{dmax2} (°C)	463	464
T_{dmax3} (°C)	715	694

3.4. Thermogravimetric Analysis (TGA). The results from the TGA and derivative thermogravimetric (DTG) tests, shown in Figure 8 along with the key data summarized in Table 4, demonstrated that both samples exhibit a fairly similar degradation profile. However, a notable disparity was observed in the initial stages of decomposition, where pure NBR began to degrade at approximately 321 °C associated with 5% weight loss, while the NGP-blended NBR exhibited an earlier onset of degradation at 229 °C. This divergence suggests that the NGP-blended sample may undergo the decomposition of Bentonite

https://doi.org/10.1021/acsomega.3c08301
ACS Omega 2024, 9, 9256−9268

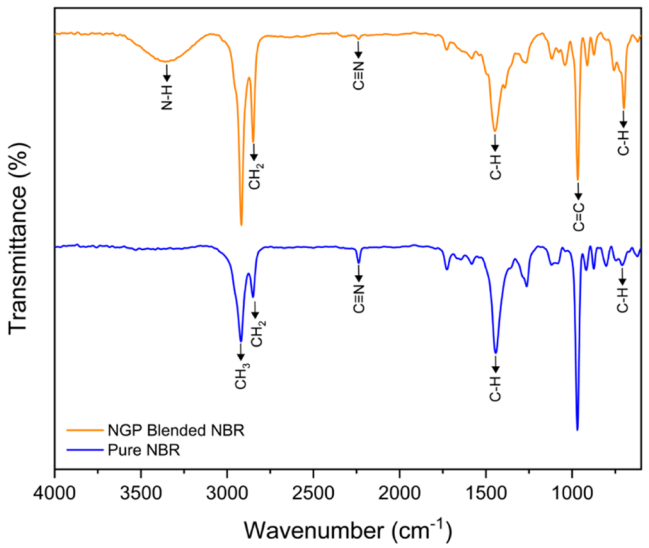

Figure 9. FTIR spectra of NBR and NBR/NGP Blend.

and iron oxide at lower temperatures, attributed to the influence of NGP[49−53]

Furthermore, a distinct decomposition point was identified in the NGP-blended NBR at approximately 307 °C, which could be linked to the decomposition of Pectin within the NGP.[54] The maximum weight loss for both samples occurred at around 464 °C, implying that the base polymer's higher content in the NGP-blended sample, compared to additives, is the primary contributor to this phenomenon. Additionally, the residual weight after decomposition revealed that pure NBR retained approximately 11.5% of its initial mass, while the NGP-blended sample retained 8%, underscoring the higher degradability of the NGP-blended sample. This aligns with the known biodegradable properties of NGP, further emphasizing the potential environmental benefits associated with incorporating NGP into NBR formulations.

3.5. Fourier Transform Infrared (FT-IR) Spectroscopy. The FTIR spectroscopy analysis was conducted to compare the spectral profiles of pure NBR and NBR blended with NGP (Figure 9). In the IR spectrum of both samples, distinct peaks were discerned, corresponding to various vibrational modes. The identified peaks included prominent ones at 2922 cm^{-1} associated with $-CH_3$ and 2851 cm^{-1} attributed to $-CH_2$ bonds.[55] A peak at 2237 cm^{-1} was associated with C≡N stretching, indicative of the nitrile groups' contribution to the polymer structure. Additionally, peaks at 1442 and 688 cm^{-1} were detected, elucidating C−H bending vibrations, while the peak at 969 cm^{-1} illustrated C═C bending vibrations.

Upon comparing the IR spectra of the NGP-blended NBR with those of pure NBR, a peak emerged at 3357 cm^{-1} in the NGP-blended NBR spectrum, indicative of N−H stretching vibrations. This finding prompts further investigation into the presence of any N−H bonds between NBR and NGP since NBR inherently lacks N−H bonds due to its nitrile (C≡N) functional groups. Notably, the intensity of the C≡N peak was lower in NGP-blended NBR than in pure NBR and the differences in the spectra between 1690 and 1640 cm^{-1} between the two samples hint at the potential formation of C═N bonds in the NGP-blended samples. Thus, the emergence of the N−H stretching peak could potentially point toward unique interactions between the NGP and the polymer matrix, leading to molecular reconfigurations or interfacial phenomena.[56]

3.6. Risk-Based Performance Analysis. Following the procedure explained in Section 2.1, a correlation between the stress response of each material and the strain% values (ε) was set using a polynomial regression (eqs 4 and 5; ($R^2 > 0.98$)). The fitted equations were then used in MC simulations, with a uniform distribution sampling over the strain levels 100−500 mm. To evaluate the superior robustness of the NGP-blended NBR compared with pure NBR, the CVaR was used to quantify the expected stress value at the worst 5% of the scenarios.

$$\text{stress (GPa)} = 0.01\varepsilon - (5.65 \times 10^{-2})\varepsilon^2 + (1.55 \times 10^{-4})\varepsilon^3; \text{ for NGP-blended NBR} \quad (4)$$

$$\text{stress (GPa)} = 0.01\varepsilon - (1.12 \times 10^{-1})\varepsilon^2 + (3.98 \times 10^{-4})\varepsilon^3; \text{ for NBR} \quad (5)$$

The ensuing probability and cumulative stress distributions are illustrated in Figure 10. Results indicated that while the stress distribution for the pure NBR is more skewed toward higher values, the CVaR of NGP-blended NBR is 80% higher. The two cumulative distribution curves were also compared via a two-way ANOVA similar to the method used in ref 57, confirming that the two distributions are statistically different (p-value < 0.05).

3.7. Aerobic and Anaerobic Biodegradability. The aerobic biodegradability test (Appendix A; Section A.4 in the Supporting Information) lasted for 60 days. Oxygen consumption in all reactors ended on day 38. The ultimate carbon releases for pure NBR-added reactors were measured as 19.71 ± 1.18 mg, for NGP-blended NBR-added reactors as 20.61 ± 0.54 mg, and for blank reactors as 22.32 ± 1.24 mg. Measured cumulative carbon release curves in the aerobic biodegradability test are given in Figure 11a, blank reactors producing slightly more CO_2 than the others indicated that there was inhibition due to the nature of the samples. NBR is known to cause inhibition on certain types of microorganisms, such as *Klebsiella pneumoniae* and *Staphylococcus aureus*.[58] Both ingredients of NBR, 1,3-butadiene[59] and acrylonitrile, were reported to inhibit microbial activity. Especially acrylonitrile, which is a type of cyanide, causes irreversible inhibition on enzyme activities of microorganisms.[60] Lönnroth[61] reported a similar cytotoxicity effect of NBR that was observed in dimethylthiazol diphenyltetrazolium, agar overlay, and filter diffusion tests. Furthermore, Yang et al.[62] reported that variations of NBR, such as carboxylated NBR, also have the potential to inhibit bacterial growth in aerobic conditions.

There was no aerobic biodegradability detected for pure NBR and NGP-blended NBR samples due to the test reactors (with samples and aerobic inoculum) producing less CO_2 than blanks (aerobic inoculum only, no sample). However, it is measured that NGP-blended NBR-added reactors produced 4.4% more CO_2 than pure NBR-added reactors, indicating lower cytotoxicity. The results showed that NGP-blended NBR is still not an ideal substrate for aerobic microorganisms to utilize, indicating biobased polymer addition to NBR has not substantially changed the material's inhibitory nature on aerobic microorganisms. Although the results of this test were not favorable for the biodegradation of the material, they showed that the material can still be used in industries where microorganism growth on the material is not desired, such as

https://doi.org/10.1021/acsomega.3c08301
ACS Omega 2024, 9, 9256−9268

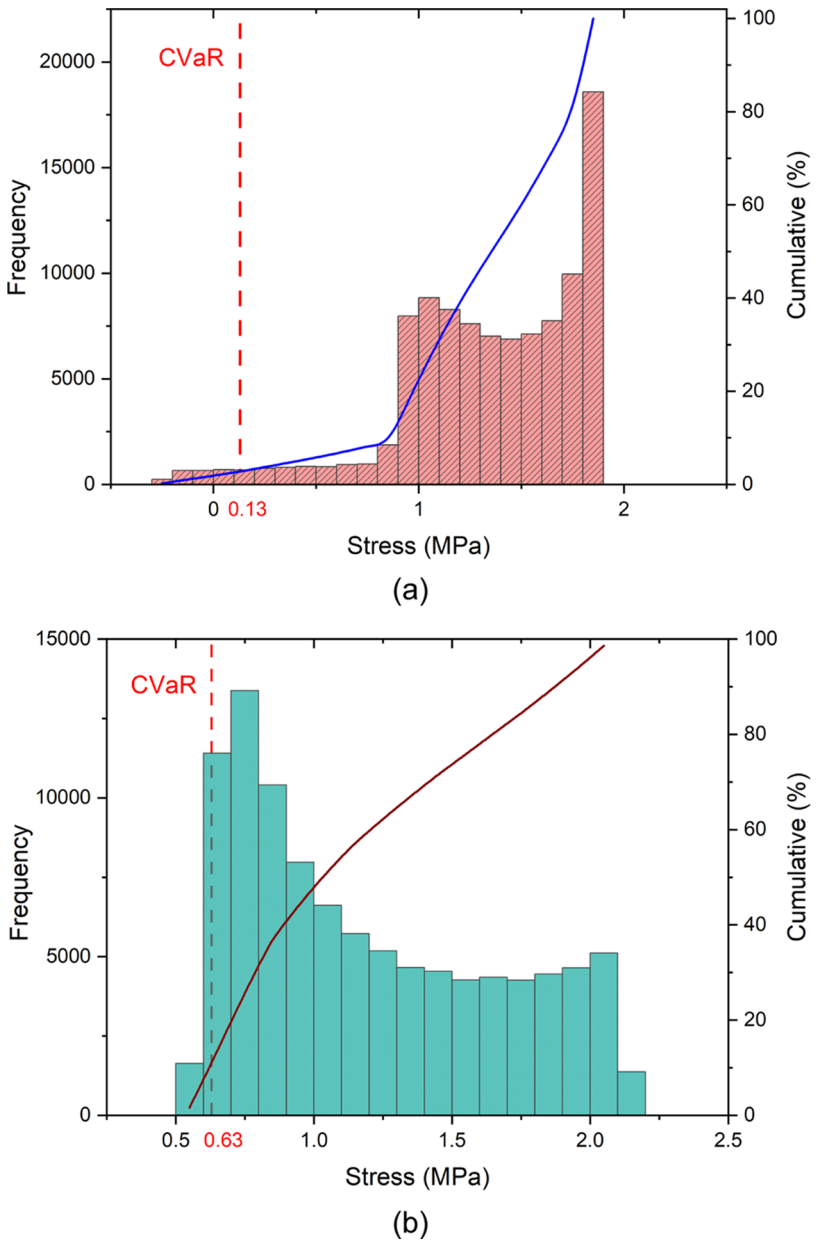

Figure 10. Risk analysis using cumulative probability distribution functions of the tensile stress response for (a) pure NBR and (b) NGP-blended NBR.

medical-grade glove production. Also, NGP-blended NBR being nonbiodegradable in aerobic conditions implies that there have been no significant changes in the mechanical properties of the material compared to pure NBR.[63]

Contrary to aerobic conditions, both NBR and NGP-blended NBR were found biodegradable in anaerobic conditions. In the anaerobic biodegradation test, carbon release, in the form of biogas,[56] was measured at 16.9 ± 0.3 mg C/g sample for NBR and 88.9 ± 3.5 mg C/g sample for NGP-blended NBR. These results represent 2.15 ± 0.03 wt % biodegradation for NBR and 11.96 ± 0.47 wt % biodegradation for NGP-blended NBR samples. Cumulative carbon release curves obtained in the anaerobic biodegradability test are given in Figure 11b. According to anaerobic digestion test results, it was found that 10 wt % NGP addition to NBR, increased biodegradability by approximately 10%. The anaerobic environment represents ideal bioreactor landfill conditions where most of the NBR products end up. Therefore, it can be said that blending NGP in NBR could bring environmental benefits due to the enhanced biodegradability it provides.

4. CONCLUSIONS

Blends of polymers/biopolymers are gaining popularity in industries because of their superior combination of mechanical performance and biodegradability characteristics. In this study, a new butadiene-acrylonitrile copolymer (NBR) and NGP blend with a 90:10 mass ratio was fabricated and investigated mechanically and environmentally. Different mechanical and characterization tests were employed to explain the different influences of the NGP additive (comprising 80 wt % base polymer, 6 wt % pectin, and other components) in comparison with the pure NBR. The experimental tests included tensile strength, tear strength, elongation at break, and resistance to

https://doi.org/10.1021/acsomega.3c08301
ACS Omega 2024, 9, 9256−9268

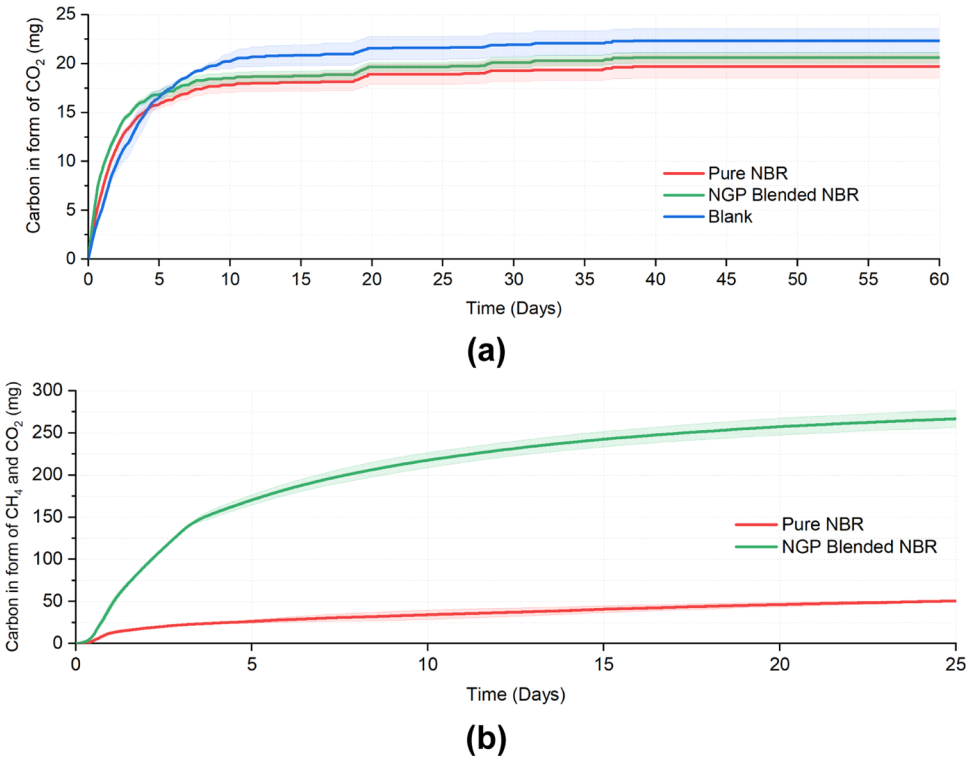

Figure 11. Biodegradability test results of NBR and NGP-blended NBR samples in (a) aerobic (blank result not subtracted) and (b) anaerobic conditions (blank result subtracted). Light colors indicate standard deviation.

puncture, followed by respirometry aerobic and anaerobic biodegradability evaluations. To analyze the functional groups and characterization of polymers in the blends, structure, and thermal properties of the NGP-blended NBR, FTIR, SEM, and TGA were performed. Moreover, the potential variability of the material blend tensile properties was evaluated using a Monte Carlo (MC)-based risk analysis to calculate the tensile strength property at the conditional value at risk.

The results demonstrated that the mechanical characteristics of the NGP-blended NBR are overall favorable to those of pure NBR. Also, given the potential uncertainties in the characterization and/or due to potential variations in loading magnitude during use, an MC simulation model was used to evaluate the Conditional Value at Risk (CVaR) of the tensile stress response of the materials. The NGP-blended NBR showed a higher (by 80%) reliability regarding worst-case performance. However, in terms of other mechanical properties, the NGP/NBR blend exhibited a lower puncture resistance compared to pure NBR coupled with higher surface roughness, likely due to imperfect adhesion of NGP to the polymer matrix.

From a biodegradability standpoint, both NBR and NGP-blended NBR were found to cause cytotoxicity on aerobic microorganisms, making them nonbiodegradable in aerobic conditions. However, under anaerobic conditions, NGP addition to NBR increased biodegradability from 2 to 12%, underscoring its more environmentally friendly attribute. Thus, the results overall indicate the potential usability of a pectin-based polymer blended with NBR to create eco-friendly materials, without compromising the mechanical performance (product quality). Future research is required to analyze the different content percentages of NGP in the NBR blend and investigate adding different compatibilizers to potentially further increase the adherence of pectin-based additives with the NBR polymer. A formal Multiple Criteria Decision-Making (MCDM) framework (e.g., see ref 64) may also be adapted to compare the performance of NGP-NBR blends under concurrent design attributes, possibly combined with a life cycle assessment.[65]

■ ASSOCIATED CONTENT

Supporting Information

The Supporting Information is available free of charge at https://pubs.acs.org/doi/10.1021/acsomega.3c08301.

Typical stress−strain behavior for polymer blends under tension at various deformation levels (Figure A1); puncture testing apparatus: a schematic of components the designed parts, manufactured fixture installed in the Instron machine (Figure A2); evaluating the puncture force incorporating friction (Figure A3); force-deflection response of the materials under puncture testing (Figure A4); biodegradability experimental setup (Figure A5); activity test result of inoculum used in the aerobic test (Figure A6); activity test result of anaerobic inoculum measured using microcrystalline cellulose (Figure A7); surface roughness parameters obtained from 3D optical microscope (Table A1); and measured thickness (mm), as used for the normalization of forces in each type of test (Table A2) (PDF)

■ AUTHOR INFORMATION

Corresponding Authors

Cigdem Eskicioglu − *Bioreactor Technology Group, School of Engineering, University of British Columbia, Kelowna, British Columbia V1V 1V7, Canada*; Email: cigdem.eskicioglu@ubc.ca

https://doi.org/10.1021/acsomega.3c08301
ACS Omega 2024, 9, 9256−9268

Abbas S. Milani − *Composites Research Network-Okanagan Laboratory, School of Engineering, University of British Columbia, Kelowna, British Columbia V1V 1V7, Canada;* orcid.org/0009-0004-4544-6855; Email: abbas.milani@ubc.ca

Authors

Niloofar Akbarian-Saravi − *Composites Research Network-Okanagan Laboratory, School of Engineering, University of British Columbia, Kelowna, British Columbia V1V 1V7, Canada*

Ibrahim Alper Basar − *Bioreactor Technology Group, School of Engineering, University of British Columbia, Kelowna, British Columbia V1V 1V7, Canada;* orcid.org/0000-0002-2104-4163

Olivia Helena Margoto − *Composites Research Network-Okanagan Laboratory, School of Engineering, University of British Columbia, Kelowna, British Columbia V1V 1V7, Canada*

Nadia Abdollahi G − *Composites Research Network-Okanagan Laboratory, School of Engineering, University of British Columbia, Kelowna, British Columbia V1V 1V7, Canada*

Bryn Crawford − *Composites Research Network-Okanagan Laboratory, School of Engineering, University of British Columbia, Kelowna, British Columbia V1V 1V7, Canada;* orcid.org/0000-0002-4480-345X

Benjamin Magel − *Composites Research Network-Okanagan Laboratory, School of Engineering, University of British Columbia, Kelowna, British Columbia V1V 1V7, Canada*

Mehrdad Gharibnavaz − *FEED Engineering Inc., Port Coquitlam, British Columbia V3C 2Z1, Canada*

Complete contact information is available at: https://pubs.acs.org/10.1021/acsomega.3c08301

Notes

The authors declare no competing financial interest.

■ ACKNOWLEDGMENTS

The research was supported by the Mitacs-Accelerate Program (grant no. IT2374) and FEED Engineering, Inc. The authors are grateful to their colleagues at the Composites Research Network for their stimulating discussions and assistance at different stages of the work. Additionally, the authors thank the Nitriflex company for providing materials in-kind and for their assistance in the processing steps.

■ REFERENCES

(1) Carvalho, A. J.; Job, A.; Alves, N.; Curvelo, A. A.; Gandini, A. Thermoplastic starch/natural rubber blends. *Carbohydr. Polym.* **2003**, *53* (1), 95−99.

(2) Riyajan, S.-A.; Sangwan, W.; Leejarkpai, T. Synthesis and properties of a novel epoxidised natural rubber-g-cassava starch polymer and its use as an impact strengthening agent. *Plast. Rubber Compos.* **2016**, *45* (6), 277−285.

(3) Fainleib, A.; Pires, R. V.; Lucas, E. F.; Soares, B. G. Degradation of non-vulcanized natural rubber - Renewable resource for fine chemicals used in polymer synthesis. *Polimeros* **2013**, *23* (4), 441−450.

(4) Tshela Ntumba, Y.-H.; Prochoń, M. The effect of modified keratin on the thermal properties of a cellulosic−elastomeric material. *J. Therm. Anal. Calorim.* **2016**, *125* (3), 1151−1160.

(5) Stelescu, M.-D.; Manaila, E.; Craciun, G.; Chirila, C. Development and Characterization of Polymer Eco-Composites Based on Natural Rubber Reinforced with Natural Fibers. *Materials* **2017**, *10* (7), 787.

(6) Sisanth, K. S.; Thomas, M. G.; Abraham, J.; Thomas, S. General Introduction to Rubber Compounding. In *Progress in Rubber Nanocomposites*; Elsevier, 2017; pp 1−39.

(7) Fazli, A.; Rodrigue, D. Recycling Waste Tires into Ground Tire Rubber (GTR)/Rubber Compounds: A Review. *J. Compos. Sci.* **2020**, *4* (3), 103.

(8) Zhang, J.; Liu, X.; Zao, W.; Feng, H.; Hou, Y.; Huo, A. High-Temperature-Aging Induced Sequential Recovery of Shape Memory Nitrile Butadiene Rubber Composites. *ACS Appl. Mater. Interfaces* **2021**, *13* (8), 10376−10387.

(9) Boukfessa, H.; Bezzazi, B. The effect of carbon black on the curing and mechanical properties of natural rubber/ acrylonitrile-butadiene rubber composites. *J. Appl. Res. Technol.* **2021**, *19* (3), 194−201.

(10) Zhang, X.; Tang, Z.; Guo, B.; Zhang, L. Enabling Design of Advanced Elastomer with Bioinspired Metal−Oxygen Coordination. *ACS Appl. Mater. Interfaces* **2016**, *8* (47), 32520−32527.

(11) Kwak, S.-Y.; Nakajima, N. Monitoring of Homogenization and Analysis of Nanoscale Structure in a Butadiene−Acrylonitrile Copolymer/Poly(vinyl chloride) Blend. *Macromolecules* **1996**, *29* (16), 5446−5452.

(12) Botros, S. H.; Younan, A. F.; Essa, M. M. Ageing and Oil Resistance of Fiber-Reinforced CR/NBR Blends. *Mol. Cryst. Liq. Cryst. Sci. Technol., Sect. A* **2000**, *354* (1), 409−420.

(13) Wimolmala, E.; Wootthikanokkhan, J.; Sombatsompop, N. Effects of composition and temperature on extrudate characteristics, morphology, and tensile properties of acrylic rubber-blended PVC. *J. Appl. Polym. Sci.* **2001**, *80* (13), 2523−2534.

(14) Daud, S.; Afiq, M. M.; Azura, A. R. Studies on the Influenced of Dextrin Filler on the Mechanical Properties of Carboxylated Nitrile Butadiene Rubber (Xnbr) Films. *J. Phys. Conf. Ser.* **2018**, *1082* (1), No. 012013.

(15) López-Mondéjar, R.; Zühlke, D.; Becher, D.; Riedel, K.; Baldrian, P. Cellulose and hemicellulose decomposition by forest soil bacteria proceeds by the action of structurally variable enzymatic systems. *Sci. Rep.* **2016**, *6* (1), No. 25279.

(16) Roy, K.; Debnath, S. C.; Pongwisuthiruchte, A.; Potiyaraj, P. Recent advances of natural fibers based green rubber composites: Properties, current status, and future perspectives. *J. Appl. Polym. Sci.* **2021**, *138* (35), No. 50866.

(17) Rayung, M.; Aung, M. M.; Azhar, S. C.; et al. Bio-Based Polymer Electrolytes for Electrochemical Devices: Insight into the Ionic Conductivity Performance. *Materials* **2020**, *13* (4), 838.

(18) Mellinas, C.; Ramos, M.; Jiménez, A.; Garrigós, M. C. Recent Trends in the Use of Pectin from Agro-Waste Residues as a Natural-Based Biopolymer for Food Packaging Applications. *Materials* **2020**, *13* (3), 673.

(19) Rodsamran, P.; Sothornvit, R. Lime peel pectin integrated with coconut water and lime peel extract as a new bioactive film sachet to retard soybean oil oxidation. *Food Hydrocolloids* **2019**, *97*, No. 105173.

(20) Sun, X.; Cameron, R. G.; Bai, J. Effect of spray-drying temperature on physicochemical, antioxidant and antimicrobial properties of pectin/sodium alginate microencapsulated carvacrol. *Food Hydrocolloids* **2020**, *100*, No. 105420.

(21) de Oliveira Alves Sena, E.; Oliveira da Silva, P. S.; de Aragão Batista, M. C.; et al. Calcium application via hydrocooling and edible coating for the conservation and quality of cashew apples. *Sci. Hortic.* **2019**, *256*, No. 108531.

(22) Lin, J.; Yu, S.; Ai, C.; Zhang, T.; Guo, X. Emulsion stability of sugar beet pectin increased by genipin crosslinking. *Food Hydrocolloids* **2020**, *101*, No. 105459.

(23) Funami, T.; Nakauma, M.; Katayama, T.; et al. Outputs through the collaborative works with Prof. G. O. Phillips on hydrocolloid emulsifiers. *Food Hydrocolloids* **2018**, *78*, 47−54.

(24) Luo, S.; Cao, J.; Sun, W. 'Evaluation of Kraft lignin as natural compatibilizer in wood flour/polypropylene composites. *Polym. Compos.* **2017**, *38* (11), 2387−2394.
(25) Mascia, L.; Su, R.; Clarke, J.; Lou, Y.; Mele, E. Fibres from blends of epoxidized natural rubber and polylactic acid by the electrospinning process: Compatibilization and surface texture. *Eur. Polym. J.* **2017**, *87*, 241−254.
(26) Mukherjee, T.; Kao, N. PLA Based Biopolymer Reinforced with Natural Fibre: A Review. *J. Polym. Environ.* **2011**, *19* (3), 714−725.
(27) Candau, N.; Oguz, O.; Federico, C. E.; Stoclet, G.; Tahon, J.-F.; Maspoch, M. L. Strain induced crystallization in vulcanized natural rubber containing ground tire rubber particles with reinforcement and nucleation abilities. *Polym. Test.* **2021**, *101*, No. 107313.
(28) Surya, I.; Ismail, H.; Azura, A. R. The comparison of alkanolamide and silane coupling agent on the properties of silica-filled natural rubber (SMR-L) compounds. *Polym. Test.* **2014**, *40*, 24−32.
(29) Nihmath, A.; Ramesan, M. T. Development of novel elastomeric blends derived from chlorinated nitrile rubber and chlorinated ethylene propylene diene rubber. *Polym. Test.* **2020**, *89*, No. 106728.
(30) Jantachum, P.; Khumpaitool, B.; Utara, S. Effect of silane coupling agent and cellulose nanocrystals loading on the properties of acrylonitrile butadiene rubber/natural rubber nanocomposites. *Ind. Crops Prod.* **2023**, *195*, No. 116407.
(31) Sinclair, A.; Zhou, X.; Tangpong, S.; Bajwa, D. S.; Quadir, M.; Jiang, L. High-Performance Styrene-Butadiene Rubber Nanocomposites Reinforced by Surface-Modified Cellulose Nanofibers. *ACS Omega* **2019**, *4* (8), 13189−13199.
(32) He, Q.; Li, Y.; Xu, J.; Zhang, C. Prediction of Mechanical Properties of Igneous Rocks Under Combined Compression and Shear Loading Through Statistical Analysis. *Rock Mech. Rock Eng.* **2020**, *53* (2), 841−859.
(33) Bekkedahl, N.; Weeks, J. J. Heats of reaction of natural rubber with sulfur. *J. Res. Natl. Bur. Stand., Sect. A* **1969**, *73A* (2), 221.
(34) Kitir, N.et al. Peat Use in Horticulture. In *Peat*; InTech, 2018.
(35) Mao, X.; Wu, B.; Zhang, F.; Wang, C.; Deng, T.; Tang, X. Synthesis and characterization of polyimide/liquid acrylonitrile-butadiene rubber composite films. *J. Mater. Sci. Mater. Electron.* **2019**, *30* (17), 16080−16086.
(36) Chakraborty, S.; Bandyopadhyay, S.; Ameta, R.; Mukhopadhyay, R.; Deuri, A. S. Application of FTIR in characterization of acrylonitrile-butadiene rubber (nitrile rubber). *Polym. Test.* **2007**, *26* (1), 38−41.
(37) Rockafellar, R. T.; Uryasev, S. Conditional value-at-risk for general loss distributions. *J. Bank Finance* **2002**, *26* (7), 1443−1471.
(38) Khadivi, M.; Sowlati, T. *Biomass Gasification Investment: A Multi-Criteria Decision Considering Uncertain Conditions*, no. 0123456789; Springer: Berlin Heidelberg, 2022.
(39) Zhou, S.; Lu, C.; Zhu, X.; Li, F. Preparation and Characterization of High-Strength Geopolymer Based on BH-1 Lunar Soil Simulant with Low Alkali Content. *Engineering* **2021**, *7* (11), 1631−1645.
(40) Wang, Y.; Zhai, W.; Cheng, S.; Li, J.; Zhang, H. Surface-functionalized design of blood-contacting biomaterials for preventing coagulation and promoting hemostasis. *Friction* **2023**, *11* (8), 1371−1394.
(41) Shah Mohammadi, M.; Ghani, M.; Komeili, M.; Crawford, B.; Milani, A. S. The effect of manufacturing parameters on the surface roughness of glass fibre reinforced polymer moulds. *Composites, Part B* **2017**, *125*, 39−48.
(42) Liu, J.; Chen, Z.; Liang, X.; et al. Puncture mechanics of soft elastomeric membrane with large deformation by rigid cylindrical indenter. *J. Mech. Phys. Solids* **2018**, *112*, 458−471.
(43) Wang, Y.; Zhai, W.; Li, J.; Liu, H.; Li, C.; Li, J. Friction behavior of biodegradable electrospun polyester nanofibrous membranes. *Tribol. Int.* **2023**, *188*, No. 108891.
(44) Zhang, Z.; Zhang, W.; Hou, Z.-W.; Li, P.; Wang, L. Electrophilic Halospirocyclization of N -Benzylacrylamides to Access 4-Halomethyl-2-azaspiro[4.5]decanes. *J. Org. Chem.* **2023**, *88* (19), 13610−13621.
(45) Botros, S. H.; Moustafa, A. F.; Ibrahim, S. A. Improvement of the homogeneity of SBR/NBR blends using polyglycidylmethacrylate-g-butadiene rubber. *J. Appl. Polym. Sci.* **2006**, *99* (4), 1559−1567.
(46) George, S. Blends of isotactic polypropylene and nitrile rubber: morphology, mechanical properties and compatibilization. *Polymer* **1995**, *36* (23), 4405−4416.
(47) Essawy, H.; El-Nashar, D. The use of montmorillonite as a reinforcing and compatibilizing filler for NBR/SBR rubber blend. *Polym. Test.* **2004**, *23* (7), 803−807.
(48) Kan, Y.; Li, J.; Zhang, S.; Gao, Z. Novel bridge assistance strategy for tailoring crosslinking networks within soybean-meal-based biocomposites to balance mechanical and biodegradation properties. *Chem. Eng. J.* **2023**, *472*, No. 144858.
(49) Zhang, G.; Zhao, Z.; Zhu, Y. Changes in abiotic dissipation rates and bound fractions of antibiotics in biochar-amended soil. *J. Clean. Prod.* **2020**, *256*, No. 120314.
(50) Yu, F.; Yu, S.; Li, C.; et al. Molecular engineering of biomimetic donor-acceptor conjugated microporous polymers with full-spectrum response and an unusual electronic shuttle for enhanced uranium(VI) photoreduction. *Chem. Eng. J.* **2023**, *466*, No. 143285.
(51) Zhang, G.; Zhao, Z.; Yin, X.-A.; Zhu, Y. Impacts of biochars on bacterial community shifts and biodegradation of antibiotics in an agricultural soil during short-term incubation. *Sci. Total Environ.* **2021**, *771*, No. 144751.
(52) Kgabi, D. P.; Ambushe, A. A. Characterization of South African Bentonite and Kaolin Clays. *Sustainability* **2023**, *15* (17), 12679.
(53) Afkari, M.; Masoudpanah, S. M.; Hasheminiasari, M.; Alamolhoda, S. Effects of iron oxide contents on photocatalytic performance of nanocomposites based on g-C3N4. *Sci. Rep.* **2023**, *13* (1), No. 6203.
(54) Kong, D.; Wilson, L. D. Uptake of Methylene Blue from Aqueous Solution by Pectin−Chitosan Binary Composites. *J. Compos. Sci.* **2020**, *4* (3), 95.
(55) Samantarai, S.; Nag, A.; Singh, N.; et al. Chemical modification of nitrile rubber in the latex stage by functionalizing phosphorylated cardanol prepolymer: A bio-based plasticizer and a renewable resource. *J. Elastomers Plast.* **2019**, *51*, 99−129, DOI: 10.1177/0095244318768644.
(56) Li, M.; Xia, Q.; Lv, S.; et al. Enhanced CO 2 capture for photosynthetic lycopene production in engineered Rhodopseudomonas palustris, a purple nonsulfur bacterium. *Green Chem.* **2022**, *24* (19), 7500−7518.
(57) Sultana, S.; Rashidi, A.; Islam, M.; Crawford, B.; Milani, A. S. Towards Reliability-Enhanced Mechanical Characterization of Non-Crimp Fabrics: How to Compare Two Force-Displacement Curves against a Null Material Hypothesis. *Open J. Compos. Mater.* **2019**, *09* (02), 164−182.
(58) Landers, T. F.; Dent, A. Nitrile versus latex for glove juice sampling. *PLoS One* **2014**, *9* (10), No. e110686, DOI: 10.1371/journal.pone.0110686.
(59) Environment Canada, 'Canadian Environmental Protection Act, 1,3-Butadiene', 1999.
(60) Alfani, F.; Cantarella, M.; Spera, A.; Viparelli, P. Operational stability of Brevibacterium imperialis CBS 489−74 nitrile hydratase. *J. Mol. Catal., B* **2001**, *11* (4−6), 687−697.
(61) Lönnroth, E.-C. Toxicity of medical glove materials: A pilot study. *Int. J. Occup. Saf. Ergon.* **2005**, *11* (2), 131−139.
(62) Yang, J.; Gao, B.; Zhang, S.; Chen, Y. Improved antibacterial and mechanical performances of carboxylated nitrile butadiene rubber via interface reaction of oxidized starch. *Carbohydr. Polym.* **2021**, *259*, No. 117739.
(63) Xu, Y.; Zhang, F.; Zhai, W.; Cheng, S.; Li, J.; Wang, Y. Unraveling of Advances in 3D-Printed Polymer-Based Bone Scaffolds. *Polymers* **2022**, *14* (3), No. 566.
(64) Milani, A. S.; Shanian, A.; El-Lahham, C. A decision-based approach for measuring human behavioral resistance to organizational

https://doi.org/10.1021/acsomega.3c08301
ACS Omega 2024, 9, 9256−9268

change in strategic planning. *Math. Comput. Model.* **2008**, *48* (11−12), 1765−1774.
(65) Milani, A. S.; Eskicioglu, C.; Robles, K.; Bujun, K.; Hosseini-Nasab, H. Multiple criteria decision making with life cycle assessment for material selection of composites. *Express Polym. Lett.* **2011**, *5* (12), 1062−1074.

https://doi.org/10.1021/acsomega.3c08301
ACS Omega 2024, 9, 9256−9268